

Has the E791 experiment measured the pion wave function profile ?

Victor Chernyak

Budker Institute of Nuclear Physics,
630090 Novosibirsk, Russia

Abstract

The cross section of hard diffractive dissociation of the pion into two jets is calculated. It is obtained that the distribution of longitudinal momenta for jets is not simply proportional to the profile of the pion wave function, but depends on it in a complicated way. In particular, it is shown that, under the conditions of the E791 experiment, the momentum distribution of jets is similar in its shape for the asymptotic and CZ wave functions, and even the ratio of the differential cross sections is not far from unity.

We argue therefore that, unfortunately, the E791 experiment has not yet measured the profile of the pion wave function. For this, the experimental accuracy has to be increased essentially.

1. The E791 experiment at Fermilab [1] has recently measured the cross section of the hard diffractive dissociation of the pion into two jets. In particular, the distribution of the total longitudinal momentum into fractions y_1 and y_2 , $(y_1 + y_2) = 1$, between jets has been measured. The main purpose was to obtain in this way the information about the leading twist pion wave function $\phi_\pi(x_1, x_2)$, which describes the distribution of quarks inside the pion in the longitudinal momentum fractions x_1 and x_2 , $(x_1 + x_2) = 1$.

The hope was based on the theoretical calculations of this cross section [2]. It has been obtained in these papers that the cross section is simply proportional to the pion wave function squared: $d\sigma/dy_1 \sim |\phi_\pi(y_1)|^2$. In such a case, it would be sufficient to measure only the gross features of $d\sigma/dy$

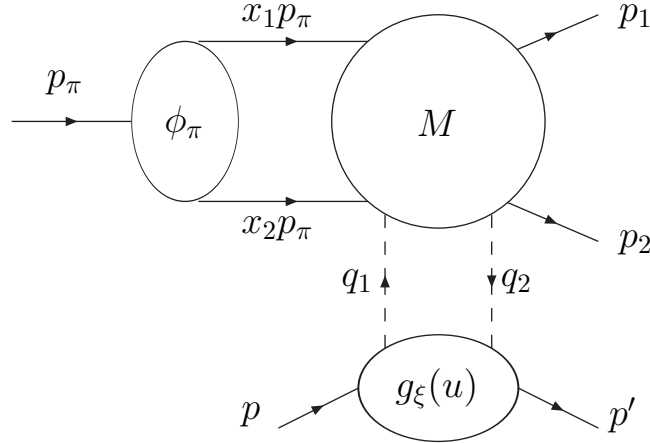


Figure 1: Kinematics and notations

to reveal the main characteristic properties of $\phi_\pi(x)$, and to discriminate between various available models of $\phi_\pi(x)$.

The purpose of this paper is to show that this is not the case and that, unfortunately, the real situation is much more complicated, with $d\sigma/dy$ depending on $\phi_\pi(x)$ in a highly nontrivial way. We give below (in a short form) the results of our calculation of this cross section.

2. The kinematics of the process is shown in fig. 1. The upper blob M represents the hard kernel of the amplitude which includes the hard gluon exchange. The two soft "external" gluons are attached in all possible ways to the hard kernel, this gives 31 Born diagrams on the whole. Two of them are represented explicitly in fig. 2 and fig. 3. The lower blob represents the (skewed) gluon structure function of the target, for which we take the nucleon.

The hard part of the amplitude can be considered as scattering of the pion on the gluon: $\pi + g_1 \rightarrow \bar{\psi}_1 + \psi_2 + g_2$. In the c.m.s. and to the leading twist accuracy, the initial and final soft gluons can be considered to be on shell, with transverse polarizations, carrying fractions $(u+\xi)$ and $(u-\xi)$ of the mean nucleon momentum \bar{P} .¹ The nucleon can be considered as being spinless, massless, and its skewed gluon distribution $g_\xi(u, t) = g_\xi(-u, t)$, $-1 < u < 1$,

¹ The small skewedness, $\xi \ll 1$, is always implied. It is typically: $\xi \sim 10^{-2}$, in the Fermilab experiment.

is defined as:

$$\begin{aligned} \langle P' | A_\lambda^{a,\perp}(v_1) A_\nu^{b,\perp}(v_2) | P \rangle &= -g_{\lambda\nu}^\perp \frac{\delta^{ab}}{8} \int_{-1}^1 du \frac{g_\xi(u, t)}{(u + \xi + i\epsilon)(u - \xi - i\epsilon)} \times \\ &\times \frac{1}{2} \left(e^{-i(u+\xi)(\bar{P}v_1) + i(u-\xi)(\bar{P}v_2)} + e^{-i(u-\xi)(\bar{P}v_1) + i(u+\xi)(\bar{P}v_2)} \right). \end{aligned} \quad (1)$$

This is equivalent to the standard definition (see [3] and [4]):

$$\begin{aligned} \langle P' | G_{\mu\lambda}^a(v_1) G_{\lambda\rho}^a(v_2) | P \rangle &= 2 \bar{P}_\mu \bar{P}_\rho \int_{-1}^1 du g_\xi(u, t) \times \\ &\times \frac{1}{2} \left(e^{-i(u+\xi)(\bar{P}v_1) + i(u-\xi)(\bar{P}v_2)} + e^{-i(u-\xi)(\bar{P}v_1) + i(u+\xi)(\bar{P}v_2)} \right). \end{aligned} \quad (2)$$

The kinematical variables are defined as:

$$q_1 = (u + \xi) \bar{P}, \quad q_2 = (u - \xi) \bar{P}, \quad \bar{P} = (P + P')/2,$$

$$\Delta = (q_1 - q_2) = 2\xi \bar{P}, \quad \xi = \frac{\mathbf{k}_\perp^2}{2y_1 y_2 s}, \quad z_1 = \frac{u + \xi}{2\xi}, \quad z_2 = \frac{u - \xi}{2\xi}, \quad (3)$$

$$z_1 - z_2 = 1, \quad 2(p_\pi \Delta) = M^2 = \frac{\mathbf{k}_\perp^2}{y_1 y_2},$$

the final quarks are on shell, carry the fractions y_1 and y_2 of the initial pion momentum, and their transverse momenta are: $(\mathbf{k}_\perp + (\mathbf{q}_\perp/2))$ and $(-\mathbf{k}_\perp + (\mathbf{q}_\perp/2))$, $|\mathbf{q}_\perp| \ll |\mathbf{k}_\perp|$, where \mathbf{q}_\perp is the small final transverse momentum of the nucleon, while \mathbf{k}_\perp is large.

According to the well developed approach to description of hard exclusive processes in QCD [5-8] (see [9] for a review), the hard exchanged gluon in all diagrams (see figs.2 and 3) has to be considered as a part of the hard kernel, not as "a tail" of the pion wave function or of the (skewed) structure function.²

² In [2] the authors tried to use the evolution equation for the pion wave function to obtain its "tail". For instance, for the asymptotic wave function it was obtained in this way: $\Psi_\pi^{asy}(x, \mathbf{k}_\perp^2, \mu) \sim \phi_\pi^{asy}(x, \mu)/\mathbf{k}_\perp^2$. It remains unclear for us how it is possible to obtain such a result from the evolution equation for the asymptotic wave function which looks as: $d\phi_\pi^{asy}(x, \mu)/d\ln \mu = \int dy V(x, y) \phi_\pi^{asy}(y, \mu) = 0$.

So, the structure of the amplitude is (symbolically):

$$T \sim \langle P | A^\perp \cdot A^\perp | P' \rangle \otimes (\bar{\psi}_1 M \psi_2) \otimes \langle 0 | \bar{u} \cdot d | \pi^- \rangle, \quad (4)$$

where the first matrix element introduces the skewed gluon distribution of the nucleon, $\bar{\psi}_1$ and ψ_2 are the free spinors of final quarks, "M" is the hard kernel, i.e. the product of all vertices and hard propagators, the last matrix element introduces the pion wave function, and \otimes means the appropriate convolution. As an example, let us consider the diagram in fig. 2. Proceeding in the above described way (see the appendix), one obtains the contribution to the amplitude (the Feynman gauge is used for the hard gluon):

$$T_2 = -\frac{16}{9} \frac{\omega_o}{y_2} \int_0^1 \frac{dx_1 \phi_\pi(x)}{x_1 x_2} \int_{-1}^1 \frac{du g_\xi(u)}{(u - \xi)(u + \xi)}, \quad (5)$$

$$\omega_o = \delta_{ij} \frac{(4\pi\alpha_s)^2}{24} f_\pi (\bar{\psi}_1 \hat{\Delta} \gamma_5 \psi_2) \frac{(y_1 y_2)^2}{k_\perp^4}, \quad \hat{\Delta} = \Delta_\mu \gamma_\mu, \quad (6)$$

where $\bar{\psi}_1$ and ψ_2 are the free spinors of the final quarks, $\Sigma_{spins} |\bar{\psi}_1 \hat{\Delta} \gamma_5 \psi_2|^2 = 2 k_\perp^4 / (y_1 y_2)$, "ij" are their colour indices, and $f_\pi \simeq 130 \text{ MeV}$ is the pion decay constant.

As it is expected that, for this process, the imaginary part of the amplitude is the main one at high energy, we have calculated only its value. For the diagram in fig. 2 this gives:

$$\text{Im } T_2 = -\frac{16}{9} \frac{2\pi s \omega_o y_1}{\mathbf{k}_\perp^2} g_\xi(\xi) \int_0^1 \frac{dx_1 \phi_\pi(x)}{x_1 x_2}. \quad (7)$$

As a final example, let us also consider the diagram in fig. 3, as it gives (together with the mirror diagram obtained by $q_1 \leftrightarrow q_2$) the logarithmically enhanced contribution $\sim \ln(s/\mathbf{k}_\perp^2)$:

$$T_3 = \frac{\omega_o}{y_1 y_2} \int_0^1 \frac{dx_1 \phi_\pi(x)}{x_1 x_2} \int_{-1}^1 \frac{du g_\xi(u) N}{(u - \xi)(u + \xi)[z_1(x_1 - y_1) - x_1 y_2]}, \quad (8)$$

$$N = [-8 z_1 z_2] + (8 y_1 y_2 - 3 - x_1 y_1 - x_2 y_2) + (z_1 + z_2)(x_1 - y_1), \quad (9)$$

$$\text{Im } T_3 = -8 \frac{\pi s \omega_o}{\mathbf{k}_\perp^2} \int_0^1 \frac{dx_1 \phi_\pi(x) g_\xi(\bar{u})}{x_1 x_2 |x_1 - y_1|} \Theta(\xi < |\bar{u}| < 1) + \dots, \quad (10)$$

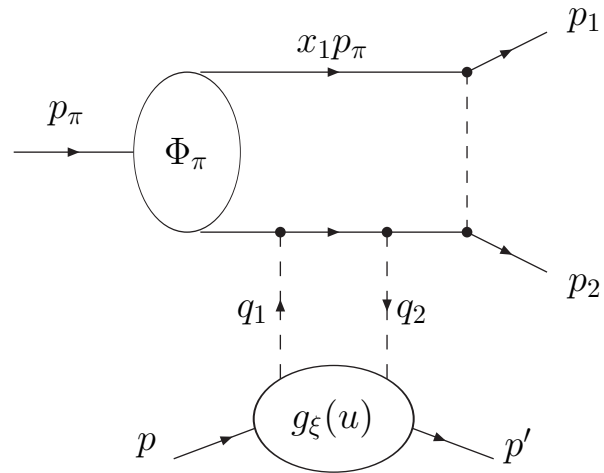


Figure 2: One of the diagrams

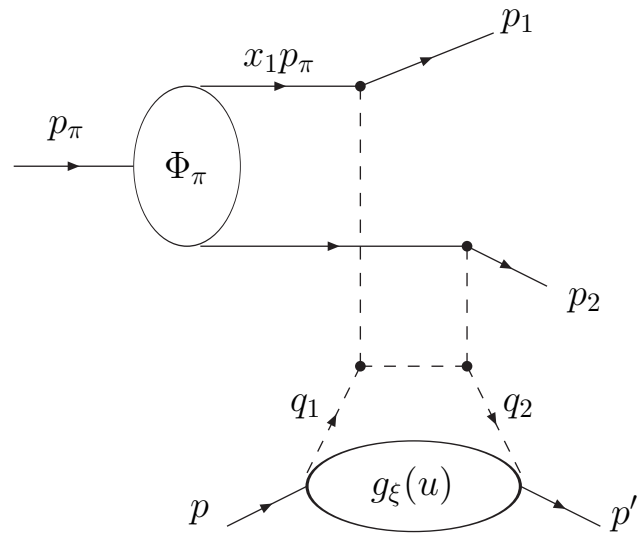


Figure 3: The diagram giving the logarithmically enhanced contribution

$$\bar{u} = \xi \left(\frac{x_1 y_2 + x_2 y_1}{x_1 - y_1} \right), \quad (11)$$

where only the logarithmically enhanced term is shown explicitly in eq.(10), which originates from the term in square brackets in eq.(9). ³

3. Proceeding in the above described way, one obtains for the cross section:

$$d\sigma_N = \frac{1}{8(2\pi)^5} \frac{1}{s^2} |T|^2 \frac{dy_1}{y_1 y_2} d^2 k_\perp d^2 q_\perp, \quad T \simeq i \operatorname{Im} T = i \frac{2\pi s \omega_o}{\mathbf{k}_\perp^2} g_\xi(\xi) \Omega, \quad (12)$$

$$\Omega = \int_0^1 dx_1 \phi_\pi(x_1) (\Sigma_1 + \Sigma_2 + \Sigma_3 + \Sigma_4), \quad (13)$$

$$\Sigma_1 = \left[-\frac{4}{x_1 x_2 |x_1 - y_1|} \frac{g_\xi(\bar{u})}{g_\xi(\xi)} \Theta(\xi < |\bar{u}| < 1) \right] + (y_1 \leftrightarrow y_2), \quad (14)$$

$$\begin{aligned} \Sigma_2 = & \frac{1}{x_1^2 x_2^2 y_1 y_2} \left\{ (x_1 x_2 + y_1 y_2) - \right. \\ & \left. - \left[|x_1 - y_1| (x_1 - y_2)^2 \frac{g_\xi(\bar{u})}{g_\xi(\xi)} \Theta(\xi < |\bar{u}| < 1) + (y_1 \leftrightarrow y_2) \right] \right\}, \end{aligned} \quad (15)$$

$$\Sigma_3 = \frac{1}{9} \left(\frac{x_1 x_2 + y_1 y_2}{x_1^2 x_2^2 y_1 y_2} \right) \left\{ 1 - \left[|x_1 - y_1| \frac{g_\xi(\bar{u})}{g_\xi(\xi)} \Theta(\xi < |\bar{u}| < 1) + (y_1 \leftrightarrow y_2) \right] \right\}, \quad (16)$$

$$\Sigma_4 = -\frac{16}{9} \frac{1}{x_1 x_2 y_1 y_2} \xi \frac{dg_\xi(u)/du|_{u=\xi}}{g_\xi(\xi)}. \quad (17)$$

The expressions (12)-(17) constitute the main result of this paper.

Let us note that while the separate terms in $\int dx \phi_\pi(x) \Sigma_2$ are logarithmically divergent at $x_{1,2} \rightarrow 0$, it is not difficult to see that the divergences

³ It is not difficult to see that the Θ - function in eq.(10) excludes the region of x_1 too close to y_1 , so that the integral is convergent and only the logarithmic enhancement $\sim \ln(s/k_\perp^2)$ remains.

cancel in the sum, so that the integral is finite. And the same is valid for Σ_3 . This is an important point, as it shows that the whole approach is self-consistent, i.e. the hard kernel remains hard and the soft end point regions $x_{1,2} \rightarrow 0$ give only power suppressed corrections.

4. In this section we present some numerical estimates of the cross section, based on the above expressions (12)-(17). Our main purpose here is to trace the distribution of jets in longitudinal momentum fractions, y_1, y_2 , depending on the profile of the pion wave function $\phi_\pi(x)$.

a) As the calculations were performed in the leading twist approximation which becomes applicable at sufficiently large k_\perp only, we take $k_\perp = 2 \text{ GeV}$. This assumes that the higher twist effects are not of great importance at such a value of k_\perp , and gives a possibility of comparison with the E791 data.

b) For the skewed gluon distribution $g_\xi(u, t)$ in the nucleon at $t \simeq -q_\perp^2 \simeq 0$ we use the simple form (as we need it at $|u| \geq \xi$ only, and because $g_\xi(u) \rightarrow g_o(u)$ at $|u| \gg \xi$):

$$g_\xi(u, t = 0, \mu \simeq |\mathbf{k}_\perp| \simeq 2 \text{ GeV})|_{u \geq \xi} \simeq u^{-0.3}(1 - u)^5. \quad (18)$$

This form agrees numerically reasonably well with the ordinary, $g_o(u, \mu \simeq 2 \text{ GeV})$, and skewed, $g_\xi(u, t = 0, \mu \simeq 2 \text{ GeV})$, gluon distributions in the nucleon calculated in [10] and [11] respectively (in the typical region of the E791 experiment: $|u| \geq \xi \sim 10^{-2}$).

The detailed consideration of nuclear effects is out the scope of this paper. So, we simply assume that these effects result mainly in an overall factor (see [2]):

$$d\sigma_A(t \simeq -q_\perp^2) \simeq d\sigma_N(t = 0) |A F_A(t)|^2, \quad (19)$$

where $F_A(t) = \exp\{bt/2\}$, $b = \langle R_A^2 \rangle / 3$, is the nuclear form factor.

c) As for the pion leading twist wave function, $\phi_\pi(x, \mu)$, we compare two model forms: the asymptotic form, $\phi_\pi^{asy}(x, \mu) = 6x_1x_2$, and the CZ-model [12]. The latter has the form: $\phi_\pi^{CZ}(x, \mu_o \simeq 0.5 \text{ GeV}) = 30x_1x_2(x_1 - x_2)^2$, at the very low normalization point. Being renormalized to the point $\mu \simeq |\mathbf{k}_\perp| \simeq 2 \text{ GeV}$, it looks as (see fig. 4):

$$\phi_\pi^{CZ}(x, \mu \simeq 2 \text{ GeV}) = 15x_1x_2[(x_1 - x_2)^2 + 0.2]. \quad (20)$$

The results of these numerical calculations are then compared with the E791 data, see fig. 5.

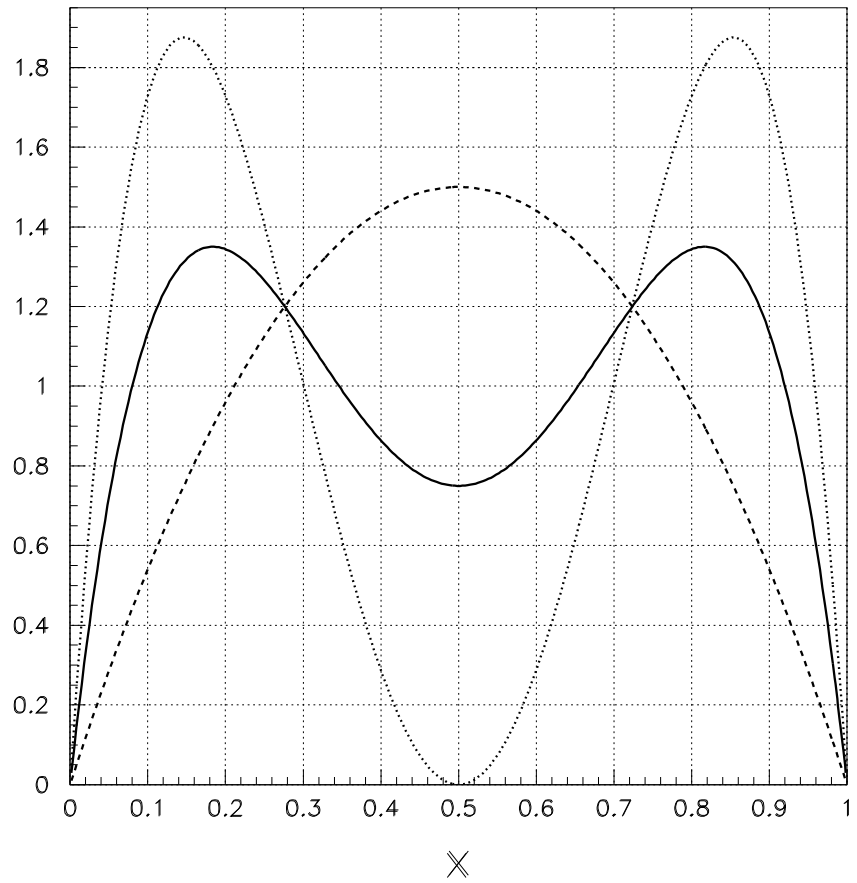


Figure 4: Profiles of the pion wave functions: a) $\phi_{\pi}^{CZ}(x, \mu \simeq 0.5 \text{ GeV}) = 30 x_1 x_2 (x_1 - x_2)^2$ - dotted line; b) $\phi_{\pi}^{CZ}(x, \mu \simeq 2 \text{ GeV}) = 15 x_1 x_2 [0.2 + (x_1 - x_2)^2]$ - solid line; c) $\phi_{\pi}^{asy}(x) = 6 x_1 x_2$ - dashed line.

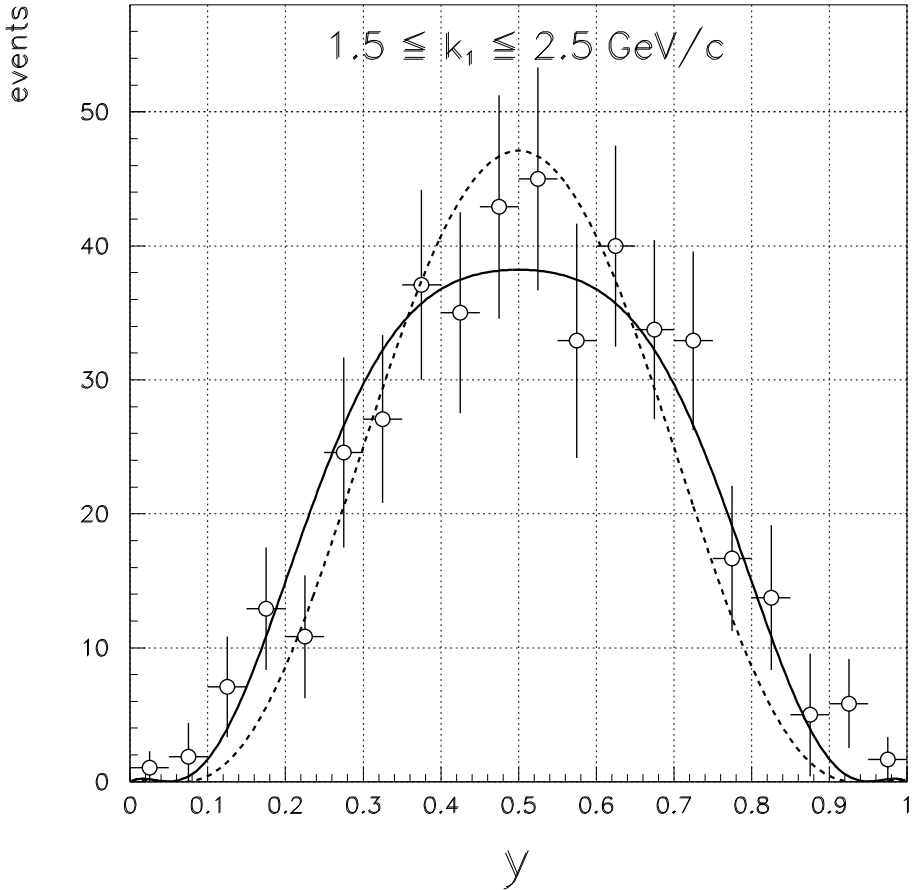


Figure 5: The y -distribution of jets calculated for $k_{\perp} = 2 \text{ GeV}$, $E_{\pi} = 500 \text{ GeV}$ and with the pion wave functions: $\phi_{\pi}^{CZ}(x, \mu \simeq 2 \text{ GeV})$ - solid line, $\phi_{\pi}^{asy}(x)$ - dashed line. The overall normalization is arbitrary, but the relative normalization of two curves is as calculated. The data points are from the E791 experiment [1].

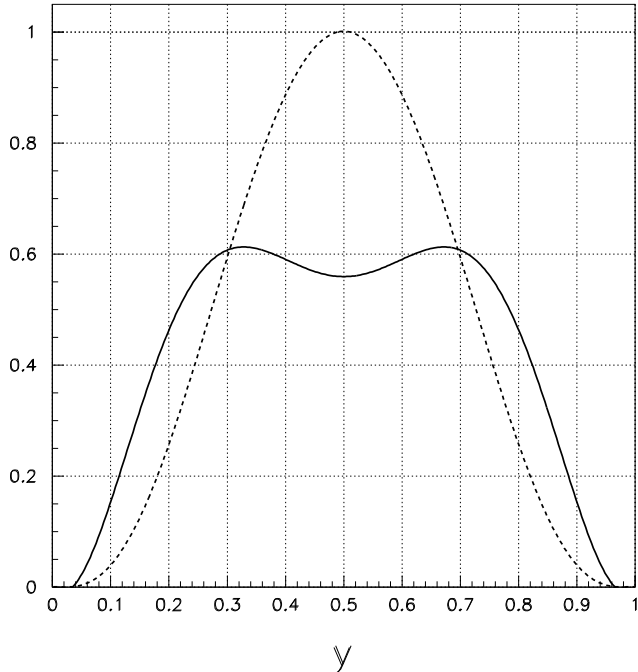


Figure 6: The same as in Fig.5, but with $E_\pi = 5 \text{ TeV}$.

It is seen that, unfortunately, while two pion wave functions are quite different, the resulting distributions of jets in longitudinal momenta are similar and, it seems, the present experimental accuracy is insufficient to distinguish clearly between them. Moreover, even the ratio of the differential cross sections is not much different from unity: $d\sigma^{asy}/d\sigma^{CZ} \simeq 1.2$ at $y_1 = 0.5$, and the same ratio is $\simeq 0.7$ at $y_1 = 0.25$.

In such an unhappy situation, the theoretical calculations should be also performed with a maximal possible accuracy (higher twist corrections, hard loop corrections, the quark structure function contribution, nuclear effects etc.).

We also show in fig. 6 the same distributions with the pion energy ten times larger, $E_\pi = 5 \text{ TeV}$, $k_\perp = 2 \text{ GeV}$. It is seen that even this does not help much (as the form of the distribution depends on the pion energy only logarithmically). The same ratios of the cross sections are here $\simeq 1.7$ and $\simeq 0.7$ respectively.

Recently the Coulomb contribution to the cross section has been calculated in [13].⁴ Its value for P_t is: $d\sigma_{P_t}^{electr}/dk_{\perp}^2 dy < 10^{-5} mbarn \cdot GeV^{-2}$, for $E_{\pi} = 500 GeV$, $k_{\perp} = 2 GeV$. Using the above given formulae, one obtains for the strong cross section at the middle point $y = 0.5$: $d\sigma_{P_t}^{CZ}/dk_{\perp}^2 dy \simeq 0.4 mbarn \cdot GeV^{-2}$ with the same parameters, and $\simeq 4 mbarn \cdot GeV^{-2}$ at $E_{\pi} = 5 TeV$. It is seen that the electromagnetic contribution is small.

Note added: After this work has been completed, the paper [14] on the same subject appeared. Comparison shows that, although the qualitative conclusions are similar, the analytic expressions for the scattering amplitude differ essentially in this paper and in [14].

Acknowledgements

I am grateful to V.S. Fadin for useful discussions and critical remarks. I also thank A.E. Bondar and B.I. Khazin for explaining me some details of the E791 experiment.

Appendix

The purpose of this appendix is to give (somewhat schematically) some details of how the diagrams have been calculated. As an example, let us consider the simplest diagram in fig.2. The momentum of the virtual gluon is: $k = (x_1 p_{\pi} - p_1)$. The momenta of virtual quarks are: $\sigma = (-x_2 p_{\pi} - z_1 \Delta)$ and $\rho = (-x_2 p_{\pi} - \Delta)$, with $q_{1,2} = z_{1,2} \Delta$, see eq.(3). The overall denominator is therefore: $D = k^2 \sigma^2 \rho^2 = (-x_1 x_2^2 y_2 z_1) (2 p_{\pi} \Delta)^3$. This diagram looks (in the operator form) as:

$$T_2 = i \frac{(4\pi\alpha_s)^2}{D} \left[\bar{d} \frac{\lambda^a}{2} \gamma_{\mu} d \right] \left[\bar{u} \frac{\lambda^b}{2} \gamma_{\lambda} \hat{\sigma} \frac{\lambda^c}{2} \gamma_{\nu} \hat{\rho} \frac{\lambda^a}{2} \gamma_{\mu} u \right] \left[A_{\lambda}^{\perp,b} A_{\nu}^{\perp,c} \right]. \quad (21)$$

The matrix element of this operator between the initial and final states is factorized then into three parts. The first part is the matrix element of the gluon fields between the initial and final nucleons, this introduces the gluon

⁴ Since the electromagnetic contribution is real, while the strong one is mainly imaginary, they do not interfere.

structure function, see eq.(1):

$$\langle P' | A_\lambda^{\perp,b} A_\nu^{\perp,c} | P \rangle \rightarrow -g_{\lambda\nu}^\perp \frac{\delta^{bc}}{8} \frac{g_\xi(u, t)}{(u - \xi)(u + \xi)}. \quad (22)$$

The second part is the matrix element of two quark fields $d_\alpha^k \bar{u}_\beta^l$ between the pion and vacuum, this introduces the pion wave function:

$$\langle 0 | d_\alpha^k \bar{u}_\beta^l | \pi^- \rangle \rightarrow \frac{\delta^{kl}}{3} \frac{(\hat{p}_\pi \gamma_5)_{\alpha\beta}}{4} i f_\pi \phi_\pi(x). \quad (23)$$

The last part is the matrix element of two remaining quark fields between the vacuum and the final state of two free quarks. This introduces the Dirac spinors $\bar{\psi}_1$ and ψ_2 . The result is integrated then over "x" and "u". So, one obtains:

$$T_2 = \int_0^1 dx_1 \int_{-1}^1 du (4\pi\alpha_s)^2 \frac{f_\pi \phi_\pi(x)}{12} \frac{g_\xi(u)}{8(u - \xi)(u + \xi)} \left(\frac{4}{3}\right)^2 \delta_{ij} (\bar{\psi}_1 M \psi_2), \quad (24)$$

$$(\bar{\psi}_1 M \psi_2) = \frac{1}{D} (\bar{\psi}_1 \gamma_\mu \hat{p}_\pi \gamma_5 \gamma_\lambda^\perp \hat{\sigma} \gamma_\lambda^\perp \hat{\rho} \gamma_\mu \psi_2) = 4 x_2 z_1 \frac{(2p_\pi \Delta)}{D} (\bar{\psi}_1 \hat{\Delta} \gamma_5 \psi_2). \quad (25)$$

On the whole, one obtains the eqs.(5,6). All other diagrams have been calculated in a similar way.

References

- [1] E.M. Aitala et. al. (E791 Collaboration), hep-ex/**0010043**
D. Ashery, hep-ex/**9910024**; Invited Talk at X Intern. Light-Cone
Meeting, Heidelberg, June 2000: hep-ex/**0008036**
- [2] L. Frankfurt, G.A. Miller and M. Strikman, Phys. Lett. **B304** (1993) 1;
Found. of Phys. **30** (2000) 533 (hep-ph/**9907214**); hep-ph/**0010297**
- [3] A.V. Radyushkin, Phys. Lett. **B385** (1996) 333; Phys. Rev. **D56** (1997)
5524
- [4] X. Ji, Phys. Rev. Lett. **78** (1997) 610; J. Phys. **G24** (1998) 1181
- [5] V.L. Chernyak and A.R. Zhitnitsky, JETP Lett. **25** (1977) 510; Sov. J.
Nucl. Phys. **31** (1980) 544

- [6] V.L. Chernyak, V.G. Serbo and A.R. Zhitnitsky, JETP Lett. **26** (1977) 594; Sov. J. Nucl. Phys. **31** (1980) 552
- [7] A.V. Efremov and A.V. Radyushkin, Phys. Lett. **B94** (1980) 245; Teor. Math. Phys. **42** (1980) 97
- [8] G.P. Lepage and S.J. Brodsky, Phys. Lett. **B87** (1979) 359; Phys. Rev. **D22** (1980) 2157
- [9] V.L. Chernyak and A.R. Zhitnitsky, Phys. Rep. **112** (1984) 173
- [10] M. Gluck, E. Reya and A. Vogt, Eur. Phys. J. **C5** (1998) 461
- [11] K.J. Golec-Biernat, A.D. Martin and M.G. Ryskin, Phys. Lett. **B456** (1999) 232; hep-ph/**9903327**
- [12] V.L. Chernyak and A.R. Zhitnitsky, Nucl. Phys. **B201** (1982) 492
- [13] D.Yu. Ivanov and L. Szymanowski, hep-ph/**0103184**
- [14] V.M. Braun, D.Yu. Ivanov, A. Schafer and L. Szymanowski, hep-ph/**0103275**